Biosensors and Bioelectronics 131 (2019) 88–94

Contents lists available at ScienceDirect

Biosensors and Bioelectronics

journal homepage: www.elsevier.com/locate/bios

Dual-signal amplification strategy for miRNA sensing with high sensitivity and selectivity by use of single Au nanowire electrodes

Haoran Tang, Jiahui Zhu, Dongmei Wang, Yongxin Li*

Anhui Key Laboratory of Chemo/Biosensing, College of Chemistry and Materials Science, Anhui Normal University, Wuhu 241000, PR China

ARTICLE INFO

Keywords:
Micro RNA
Dual-signal amplification strategy
Single Au nanowire electrodes
Nanosensors

ABSTRACT

MicroRNAs (miRNAs) have been applied as biomarkers and better detection of their expression profiles plays important roles in early diagnosis of cancers. In this work, a simple dual-signal amplification strategy has been used to construct a novel nanosensor on single Au nanowire electrodes (SAuNWEs) for miRNA-16 detection based on the "signal-on" and "signal-off" features during hybridization/de-hybridization process. The ferrocene-labeled aptamer capture probe (Fc-CP-16) is designed to hybridize with thiolated methylene blue-labeled DNA probe (MB-CP) on SAuNWE to form duplex DNA, and the addition of miRNA-16 can lead to the dissociation of duplex structure due to the highly matched sequences between miRNA-16 and Fc-CP-16. The remaining MB-CP can thus tend to recover its hairpin structure at the presence of Mg^{2+} through the hybridization of its complementary sequences. During this hybridization/de-hybridization process, the changes of Fc and MB oxidation peaks can be recorded, and there has a linear relationship between the sum of dual-signal changes ($\Delta I = \Delta I_{MB} + |\Delta I_{Fc}|$) and the logarithm of miRNA-16 concentrations, which can be used to detect miRNA-16. Including miRNA extraction, the dual-signal amplification strategy for miRNA sensing assay was carried out about 2 h for the detection in real samples. This novel nanosensor has small dimension, good selectivity, rapid response and regeneration ability, which can satisfy the need for early cancer marker detection in cells/organelles.

1. Introduction

MicroRNAs (miRNAs) are a kind of single-stranded, endogenous and non-protein coding RNAs with ~ 19–25 nucleotides, which play important roles in many biological processes (Dong et al., 2013). It has been demonstrated that the aberrant (up-/down-regulated) expressions of miRNAs are always related to various cancers (Kakkassery et al., 2017; Laterza et al., 2009). Therefore, miRNA expression profiles can be employed as effective biomarkers for molecular diagnosis of tumors (Chen et al., 2008; Coulouarn et al., 2009). For miRNA detection, classic quantitative reverse transcription polymerase chain reaction (Qrt-PCR) and microarray methods are the mainstream techniques for analysis of miRNAs in plasma or serum, but the shortages of time-consuming process and high-cost have limited its applications (Liu et al., 2004; Thomson et al., 2004; Yuen et al., 2002). The northern blotting method, based on size separation of RNA samples and detection using optical/radioactive probes, is a time-/sample-consuming technique with low sensitivity, which has also limited its applications in routine miRNA analysis (Weiss et al., 2009). Recently, several optical (fluorescence and chemiluminescence) and electrochemical methods for miRNA detection have been developed based on signal amplification strategies using nanomaterials/nucleases (Feng et al., 2018; Liu et al., 2017; Miao et al., 2018; Qian et al., 2016; Shi et al., 2015; Wang et al., 2015; Yang et al., 2014; Yu et al., 2018). However, challenges for detection of miRNA, especially in living system or limited volume/quantity samples, are still existed due to their low abundance and similar sequence among family members (Sassolas et al., 2008; Wang et al., 2015).

Nanoelectrodes (radius < 100 nm) have attracted wide interest due to their remarkable advantages, such as smaller RC constant, high mass-transport rate, and the reduced effect of solution resistance (Katemann and Schuhmann, 2002; Li et al., 2009; Shao et al., 1997; Zhang et al., 2004, 2006). Incorporation of micro-/nano-electrodes in sensor fabrication has its obvious advantages for analysis of samples with confined quantity/volume or for samples in-vivo (Actis et al., 2014; Hua et al., 2018a; Wang et al., 2015). The miniaturized nanosensors have been used in bio-analysis, for example, Zhang's group (Jena et al., 2010) and Lai's group (Salamifar and Lai, 2014) used single Au nanodisk electrodes for ferrocene counting and DNA sensing by electrodeposition of gold wire inside nanopore, Schuhmann's group (Actis et al., 2014;

* Corresponding author.
E-mail address: yongli@mail.ahnu.edu.cn (Y. Li).

https://doi.org/10.1016/j.bios.2019.02.023
Received 30 October 2018; Received in revised form 15 January 2019; Accepted 1 February 2019
Available online 19 February 2019
0956-5663/

Marquitan et al., 2016) and Mirkin's group (Li et al., 2017; Wang et al., 2012) fabricated Prussian blue/Pt modified nanoelectrodes for detecting reactive oxygen and nitrogen species inside cells/tissues, and we also developed gold nanoelectrodes-based nanosensor for ATP detection (D. Wang et al., 2018). Most of the works mentioned above for target detection, even single-molecule detection are used the special property of nanoelectrodes such as small dimension (e.g. nanodisk, nanowire, and nanogap) and fast response (Jena et al., 2010; Sun and Mirkin, 2008; D. Wang et al., 2018). However, application of micro-/nano-electrodes for miRNA detection is rare, which may be due to the low response signal because the surface area of nanoelectrodes is relatively small and the abundance of miRNA in samples is pretty low.

Herein, we developed a novel electrochemical nanosensor for the detection of miRNA-16 as a model target through a dual-signal amplification strategy (Deng et al., 2017; Xiang et al., 2017). The miRNA-16 is a unique sequence that is expressed in liver, breast, and lung, etc., and the aberrant expression levels can be used to determine clinical prognosis (Schetter et al., 2008). This nanosensor was fabricated on single Au nanowire electrodes (SAuNWEs), which were prepared by laser-assisted pulling process developed by our lab (Hua et al., 2018b; H. Wang et al., 2018; Zhang et al., 2015, 2017) and other groups (Liu et al., 2015; Salamifar and Lai, 2014; Velmurugan et al., 2009). The fabrication process of nanosensor was illustrated as Scheme 1. The thiol-modified hairpin capture probe with methylene blue tags (**MB-CP**) were self-assembled on SAuNWE surface through the formation of Au–S bond, and the excess active sites were then blocked with 6-mercaptohexanol (MCH). Then **MB-CP** modified SAuNWE hybridized with ferrocene (Fc) labeled aptamer probe (**Fc-CP-16**) through complementary pairing of base pairs to form a double-stranded structure, in which both MB and Fc were employed as electroactive species and had significant contributions to the response signal of miRNA-16. At the duplex structure, Fc was confined close to electrode surface and an intense electrochemical signal could be observed (**curve a**, E_p = 0.17 V), whereas MB was kept relatively far from electrode surface and the electron transfer between the MB and the electrode was hindered due to steric hindrance (**curve b**, E_p = −0.28 V). In our design, **MB-CP** and **Fc-CP-16** are not perfectly matched, their duplex structure can be uncoupled by a more highly matched target (miRNA-16). When the duplex structure modified SAuNWE was hybridized with miRNA-16 solution, **Fc-CP-16** dissociates from the duplex structure into solution, Fc was closed to electrode surface and the reduction signal increased significantly (**curve b**), and the **MB-CP** would bent to form the stem-loop structure in the $MgCl_2$ solution (Wu et al., 2013), For miRNA-16 detection, we can monitor the MB signal enhancement and Fc signal suppression, and there have both "turn-on" and "turn-off" signal changes. We used the sum of increased MB current peak and decreased Fc current peak as our final response ($\Delta I = \Delta I_{MB} + |\Delta I_{Fc}|$), and dual-signal amplification strategy for miRNA detection with high sensitivity

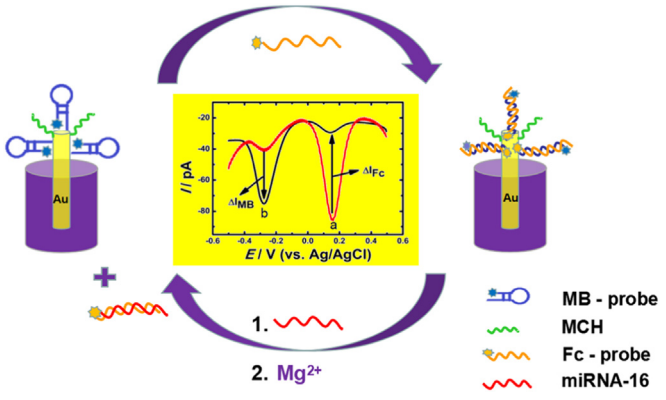

Scheme 1. Schematic illustration of the Dual-signal strategy for miRNA-16 detection.

could be realized. Compared to other miRNA detections, the proposed method using dual-signal amplification strategy exhibits high sensitivity, fast response, and good selectivity. More importantly, from the satisfactory result for detection of miRNA-16 extracted from human breast cancer cells (MCF-7) and considering the small dimensions, this nanoelectrode-based sensor it can satisfy the need for early cancer marker detection in cells/tissues.

2. Experimental section

2.1. Chemicals and materials

The following chemicals were used as received: potassium chloride (KCl, Mallinckrodt Baker), hexaammineruthenium (III) chloride ($(Ru(NH_3)_6Cl_3$, Aldrich), 1-ferrocenylethanol (FcMeOH, Aldrich), ferrocene (Fc, Aldrich), potassium ferricyanide ($K_3Fe(CN)_6$, Acros Organics), sodium chloride (NaCl, Sangon Biotech, China), hydrofluoric acid (HF, Shanghai Sinopharm, China), acetonitrile (ACN, Sangon Biotech), acetic acid (CH_3COOH, Acros Organics), tetra-*n*-butylammonium hexafluorophosphate ($TBAPF_6$, Aldrich), sodium acetate (CH_3COONa, Mallinckrodt Baker), sulfuric acid (H_2SO_4, EMD Chemicals Inc., China), Magnesium chloride ($MgCl_2{\cdot}6H_2O$, Aldrich), 6-mercaptohexanol (MCH, Shanghai Chemical Co. Shanghai, China), dithiothreitol($C_4H_{10}O_2S_2$, DTT, Aldrich), phosphate buffer consists of sodium hydrogen phosphate and sodium dihydrogen phosphate (Shanghai Ling Feng Chemical Reagent Co., Ltd., Shanghai, China). HPLC-purified DNA and miRNAs oligonucleotides were purchased from Sangon Biotech Co. Ltd (Shanghai, China). The sequences of the oligonucleotides are listed in Table S1. All reagents were analytically pure grade. Aqueous solutions were prepared using ultrapure water (specific resistance of 18 MΩ cm). Unless otherwise noted, all PBS solution used in the experiments to follow were 0.01 M of pH 7.5 PBS.

25 μm diameter Au microwires (99.95%, hard) and 250 μm tungsten (99.99%) were purchased from Alfa-Aesar. Glass capillaries (*i.d.* = 0.64 mm, *o.d.* = 1.0 mm) were purchased from Sutter Instrument Co. The silver-filled epoxy glue was bought from DuPont Lt. Co. The nanoelectrodes were firstly polished with finer grit sandpapers (400 W, 800 W, and 1200 W grits, Shanghai Chemical Co., Shanghai) and alumina polishing powders (1.0, 0.3, and 0.05 μm, Buehler).

2.2. Cell culture and total miRNA extraction

The human breast cancer cells (MCF-7) were obtained from the cell bank of the type culture collection of the Chinese Academy of Sciences (Shanghai, China) and cultured in RPMI 1640 medium (Thermo Scientific Hyclone) supplemented with 15% fetal bovine serum, 100 U mL^{-1} penicillin, and 100 μg mL^{-1} streptomycin. Cells were all cultured at 37 °C in a humidified incubator containing 5% CO_2. Total miRNA was extracted from MCF-7 cells (~10^6 cells) by Total RNA Extractor (Sangon Biotech, Shanghai, China) according to the manufacturer protocols. The final supernatant was diluted with RNase-free water. The extract was stored at −20 °C for future use.

2.3. Instruments

A laser-assisted puller (P-2000 mode, Sutter Instrument Co., Novato, CA) was used for the fabrication of gold nanotips. OLYMPUS bio-optical microscope (BX53 + DP72, Japan) was used to check the nano-tips after pulling. TEM images of single Au electrodes were obtained from a Tecnai G2 F20 (FEI) microscope and no additional coatings were performed prior to imaging. The electrochemical experiments were performed with a CHI 650e electrochemical workstation (Chenhua Instrument Co., Shanghai, China). All experiments were carried out with a three-electrode system consisting of a Ag/AgCl reference electrode, platinum wire as an auxiliary electrode, and single Au nanoelectrode as a working electrode. All experiments were carried out at

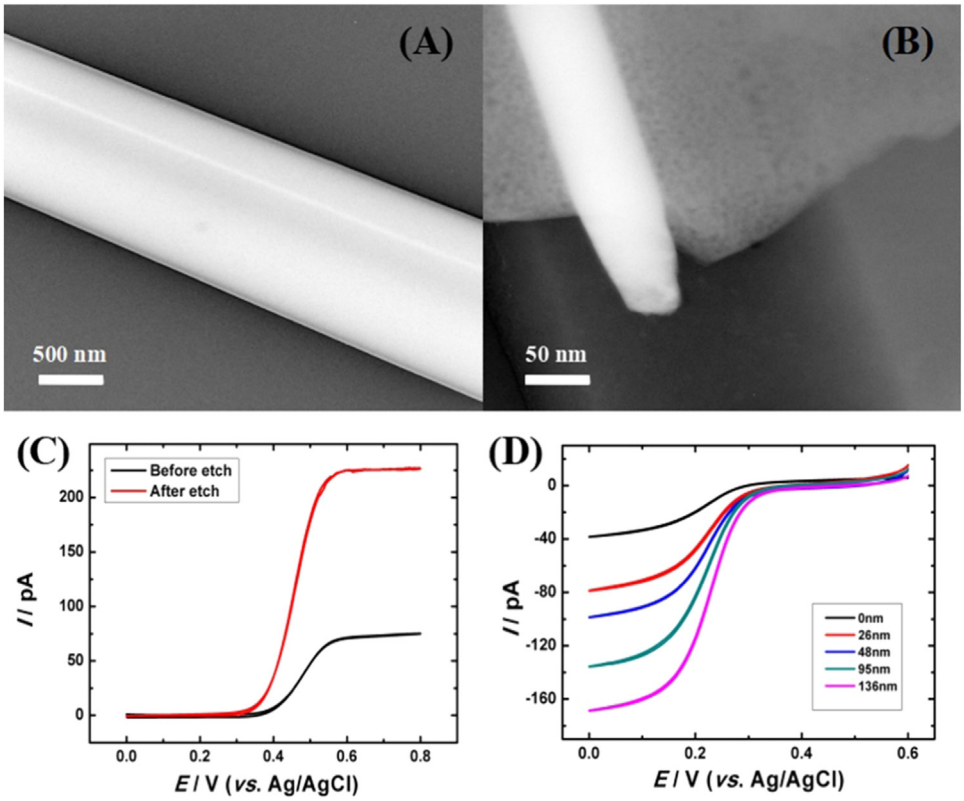

Fig. 1. (A), (B) TEM images of single Au nanowire electrode with different magnification. (C) CVs of single Au nanodisk electrode before (black curve) and after (red curve) HF etching in a 5.0 mM Fc ACN solution containing 0.2 M $TBAPF_6$. Radius, 15 ± 3 nm. (D) Voltammetric responses of single Au nanowire electrodes in a 5 mM $K_3Fe(CN)_6$ solution containing 0.2 M KCl. Scan rate, 20 mV/s (For interpretation of the references to color in this figure legend, the reader is referred to the web version of this article.).

room temperature.

2.4. Preparation of single Au nanowire electrodes

The SAuNWEs were prepared from single gold nanodisk electrodes, which were prepared by laser-assisted pulling process developed by us (Zhang et al., 2015, 2017) and other groups (Liu et al., 2015; Salamifar and Lai, 2014; Velmurugan et al., 2009). Briefly, a 25 μm diameter gold wire was sealed into a glass capillary (*i.d.* = 80 μm, *o.d.* = 300 μm) and then pulled by a laser-assisted puller. The pulled ultra-sharp tip was inserted into a large glass tube (*i.d.* = 0.64 mm, *o.d.* = 1.0 mm,) carefully using a hydrogen flame under vacuum, and then polished with sandpapers/alumina powders under the monitor of a home-made tester. After that, the obtained single gold nanodisk electrode was etched in a HF aqueous solution (1:4, v/v) at different time (Li et al., 2013), and the SAuNWEs with different lengths were prepared.

2.5. Preparation of RNA sensors

First of all, the disulfide bond of the MB-CP (MB-SH) was reduced with dithiothreitol (DTT) and then DTT was removed by ethanol. The specific steps are as follows. First, the oligonucleotide (MB-SH) was dissolved in 100 μL water after centrifugation. At the same time, 4 mg DTT was added into 100 μL tris-HCl buffer (0.1 M, 100 mM NaCl, pH 8.5) and incubated in the dark for 1 h, which was called as reducing agent. After that, the reducing agent was added into the target primer (MB-SH) and standing for 3 h. Then, the reduced primers were added to the mixed solution containing 200 μL acetic acid (6%), 50 μL sodium acetate (3.0 M) and 1.6 mL ethanol (100%), and the solution was centrifuged at high speed for 5 min to remove supernatant and dried for use.

The SAuNWE was cleaned by potential scanning in a 0.5 M H_2SO_4 solution from -0.3V to 1.5 V at the scan rate of 0.1 V/s until the typical characteristic peak appeared. The **MB-CP** was solubilized with 0.01 M PBS (pH 7.5) and diluted to 2.0 μM. For immobilization, the cleaned SAuNWE was immersed into **MB-CP** solution and incubated for 12 h at 37 °C in the dark to obtain the **MB-CP** modified SAuNWE and a stem-loop structure was formed. After that, the electrode was immersed into 2 mM MCH with 10 mM tris-HCl buffer for one hour to block the uncovered gold surface. The **MB-CP** modified SAuNWE was properly cleaned and then immersed in 0.2 μM of **Fc-CP-16** solution (containing 0.01 M PBS, 140 mM NaCl and 5 mM $MgCl_2$) at 37 °C for 2 h. The **Fc-CP-16** can hybridize with the **MB-CP**, resulting in the stem-loop structure of **MB-CP** unfolded and forming a relatively stable duplex structure.

2.6. Electrochemical detection of miRNA-16

The 200 μL of target molecules (miRNA-16, 10 mM PBS, 100 mM NaCl, pH 7.5) with different concentrations were incubated with **Fc-CP-16/ MB-CP** modified SAuNWE for 1 h at 37 °C to verify the feasibility of proposed miRNA nanosensor. After incubation, the nanosensors were rinsed with water and bathed in buffer with high ionic strength (0.01 M PBS containing 140 mM NaCl and 5 mM $MgCl_2$, pH 7.5) for 10 min at room temperature, which led to the formation of stem-loop structure of **MB-CP** on electrode surface. Electrochemical measurements were performed on a CHI 660D electrochemistry workstation (Chenhua Instrument Company of Shanghai, China) with a three-electrode system, including a Ag/AgCl electrode as the reference electrode, a platinum wire as the counter electrode, and modified SAuNWE as the working electrode. Square wave voltammetry (SWV) were carried out in PBS with a step potential of 4 mV, a frequency of 25 Hz, and an amplitude of 25 mV over the range from −0.5 V to + 0.5 V.

After miRNA detection, the nanosensor was regenerated by incubating with 200 μL of 0.2 μM **MB-CP** solution. Selectivity tests of the nanosensor were carried out through matched with a series of mismatched RNAs, and two natural miRNAs (miRNA-15, miRNA-21) which always coexisted with miRNA-16.

3. Results and discussion

3.1. Electrochemical performance of SAuNWEs

SAuNWEs were prepared by etching single Au nanodisk electrodes with hydrofluoric acid, and the single Au nanodisk electrodes were fabricated by laser-assisted pulling technique developed by our lab (Zhang et al., 2015, 2017) and other groups (Liu et al., 2015; Salamifar and Lai, 2014; Velmurugan et al., 2009). The pulled Au nanotip was checked firstly using TEM, and Fig. 1**A** showed clearly that a gold wire with the radius of 20 nm was sealed inside a glass capillary very well. After HF etching, gold wire was exposed and no obvious gap appeared between gold nanowire and glass sheath (Fig. 1**B**). The voltammetric responses of single Au nanodisk electrode before and after HF etching were recorded in a 5.0 mM Fc ACN solution containing 0.2 M $TBAPF_6$ (Fig. 1**C**), which clearly showed that both of the cyclic voltammograms were well-defined sigmoidal shape and low charge current, only the steady-state limiting current was significantly increased after HF etching. Based on the derivations developed by Bard et al., the dimensions of the Au nanodisk electrodes and nanowire electrode can be calculated as follows (Bard and Faulkner, 2001):

$$i_d = 4nFDC_b a \tag{1}$$

$$i_{qss} = \frac{2nFADC_b}{r_0 \ln \tau} \tag{2}$$

where i_d and i_{qss} are steady-state limiting current from CVs of nanodisk and nanowire electrode, respectively. n is the number of electrons transferred per mole of molecules, F is the Faraday constant, D is the diffusion coefficient, C_b is the concentration of the redox species, a is the radius of nano-disk electrode, and A is the surface area of the nanowire electrode, and r_0 is the radius of SAuNWE. $\tau = 4Dt/r_0^2$, where t is the time component, which can be predicted as $t = (RT/Fv$, v is the potential scan rate). According to the COMSOL simulation (Figs. S1 and S2, Supporting information) (Zhang et al., 2015, 2017), the radius of SAuNWE showed in Fig. 1**C** is 15 ± 3 nm and the length is 40 ± 5 nm. The SAuNWEs with different wire lengths (0 nm, 26 nm, 48 nm, 95 nm, and 136 nm) were obtained by changing the etching time in HF solution and their electrochemical behaviors in different redox species, including $K_3Fe(CN)_6$ (Fig. 1**D**), Fc (Fig. S3), $FcCH_2OH$ (Fig. S4), and $Ru(NH_3)_6Cl_3$ (Fig. S5), were investigated. From the well-defined sigmodal shape and low charge current shown above, it can be obtained that the SAuNWEs are fabricated successfully.

3.2. Fabrication of RNA nanosensor

The process of fabricating nanosensors were recorded with square wave voltammetry (SWV) as shown in Fig. 2. The thiol-modified SH-CP hairpin capture probe with methylene blue (**MB-CP**) tags were self-assembled on SAuNWE through the formation of Au–S bond to fabricate the **MB-CP**/SAuNWE, and the excess active sites were then blocked with MCH. During this incubation process, **MB-CP** can be preconcentrated and immobilized on SAuNWE surface. As shown in Fig. 2**A**, there was a significant current peak near −0.28 V because of the efficient electron transfer between the **MB-CP** with SAuNWE. The amount of MB-probe immobilized on SAuNWE can be calculated by Faraday's laws of electrolysis as follows,

$$n = \frac{Q}{ZF} \tag{3}$$

where n is the amount of MB-probe immobilized on SAuNWE, Q is the charge associated with the voltammetric peak, Z is the number of electrons transferred per redox molecule, and F is the Faraday constant. As shown in Fig. 2**A**, the charge from MB reduction peak area can be obtained to 4.7×10^{-12} C. On the basis of Eq. (3), the amount of MB-probe was calculated to be 4.9×10^{-17} mol, which can convert into the MB-probe molecules as 2.9443×10^7. The surface coverage of MB-probe on SAuNWE can be easily computed by the following equation (Jena et al., 2010):

$$\Gamma^* = \frac{Q}{ZFA} \tag{4}$$

where Γ^* is the surface coverage of MB-probe, Q is the charge associated with the voltammetric peak, Z is the number of electrons transferred per redox molecule, F is the Faraday's constant, and A is the area of the Au nanoelectrode, respectively. From the above, the surface coverage of MB-probe on the Au nanowire electrode showed in Fig. 2**A** is 4.3×10^{14} molecules per cm^2, which is slightly larger than the value reported previously (Chidsey et al., 1990), probably due to the surface roughness of single Au nanoelectrode. It is must be pointed out that the surface area in Eq. (4) is called as “effective surface area”, which can be calculated as 6.8×10^{-12} m^2 from the reduction peak of CV in H_2SO_4 solution (shown in Fig. S6, Supporting information), which is 704-fold larger than its geometric surface area (Salamifar and Lai, 2014).

The **MB-CP** modified SAuNWE and **Fc-CP-16** with ferrocene (Fc) tags hybridized through complementary pairing of base pairs to fabricate **Fc-CP-16**/**MB-CP**/SAuNWE. The hairpin structure was opened to form a duplex structure and electron transfer between the MB on **MB-CP** and the electrode was hindered due to steric hindrance. As shown in Fig. 2**B**, the peak of MB at −0.28 V decreased greatly and a significant current peak appeared near 0.17 V due to Fc oxidation on **Fc-CP-16**. However, **MB-CP** and **Fc-CP-16** are not perfectly matched, their double helix structure is unstable and can be uncoupled by a more highly matched target (miRNA-16). The **Fc-CP-16**/**MB-CP**/SAuNWE was hybridized with 0.1 μM of miRNA-16 solution for 1 h, which resulted in the duplex structure uncoupled due to the perfect match between miRNA-16 and **Fc-CP-16**. And then, **MB-CP** were bent to form the stem-loop structure at the presence of $MgCl_2$ (Wu et al., 2013), the MB signal at −0.28 V was recovered, and the Fc signal at 0.17 V was reduced greatly (shown in Fig. 2**C**). This performance indicated that the nanosensor we prepared have sensitive responses to miRNA-16. In the presence of miRNAs, there are both "turn-on" and "turn-off" signal changes. The signal sum of the increased MB current peak and the decreased Fc current peak was used as our final response ($\Delta I = \Delta I_{MB} + |\Delta I_{Fc}|$), and dual-signal amplification strategy for miRNA detection with high sensitivity was realized.

3.3. miRNA assay by use of nanosensor

The prepared nanosensor has been used to investigate the analytical performance for miRNA-16 detection. Fig. 3**A** provides the SWV responses of nanosensor after being treated with different concentrations of miRNA-16. It can be clearly observed that Fc signal at ~0.17 V decreases and the MB signal at ~ −0.28 V increases gradually with the increase of miRNA-16 concentrations. The resulting calibration plots are given in Fig. 3**B**, which shows that both signals of Fc and MB are linear to the logarithm of the target concentration (miRNA-16) from 0.1 pM to 100 nM. The linear regression equations are ΔI_{MB} (pA) $= 120.4 + 8.69 \lg C_{miRNA}$ (M, $R^2 = 0.9989$) and ΔI_{FC} (pA) $= -176.0 - 12.37 \lg C_{miRNA}$ (M, $R^2 = 0.9912$) for the oxidation of MB and Fc, respectively. The detection limits (LOD, S/N = 3) can be calculated as 43 fM for MB signal and 24 fM for Fc signal, respectively. To further amplify the SWV response, “$\Delta I_{MB} + |\Delta I_{Fc}|$” is used as the response signal to assay miRNA-16 quantitatively, and a linear relationship between ΔI ($\Delta I_{MB} + |\Delta I_{Fc}|$) and lg C_{miRNA} can also be obtained (shown in Fig. 3**C**). The corresponding linear regression equation is ΔI (pA) $= 296.38 + 21.06 \lg C_{miRNA}$(M)($R^2 = 0.9916$) with the detection limit of 16 fM, indicating that the dual-signal amplification strategy has lower LOD than that using ΔI_{MB} or ΔI_{FC} as response signal, and the linear range and LOD are much better than other sensing methods developed previously (see Table S2) (Eksin and Erdem, 2018; Erdem and Congur, 2014; Frascella et al., 2015; Gao et al., 2018; Poehlmann and

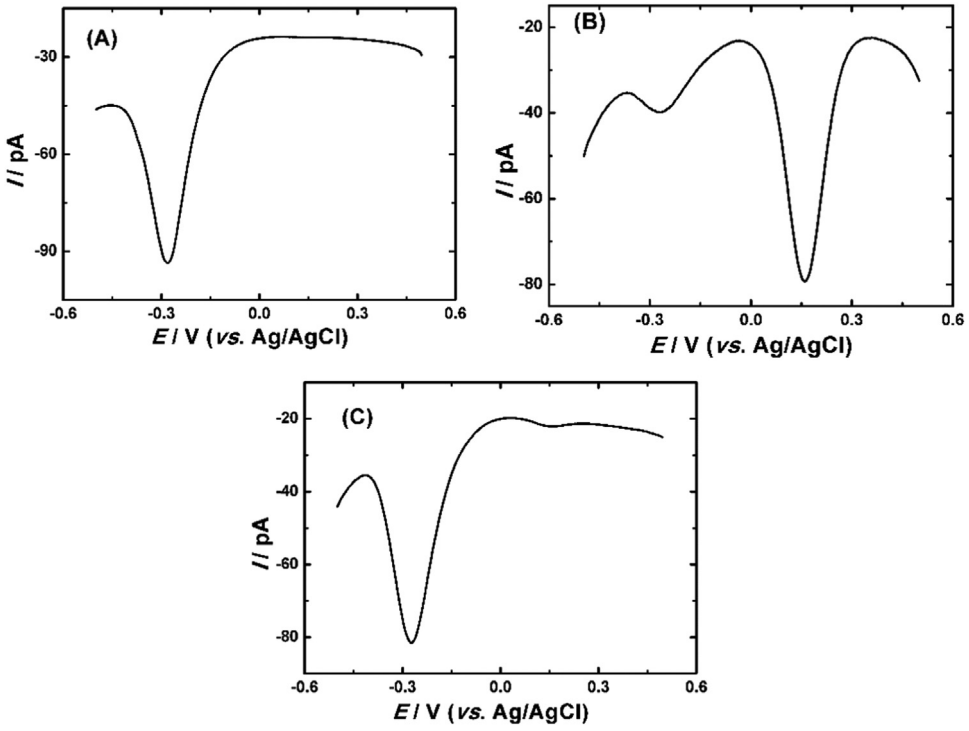

Fig. 2. The SWV responses of SAuNWE modified with **MB-CP** (A), **Fc-CP-16** and **MB-CP** (B) and after hybridization with 0.1 μM target miRNA-16 (C) in a 0.01 M PBS solution. Radius, 28 ± 5 nm; length, 41 ± 4 nm.

Sprinzl, 2010).

3.4. Selectivity, regeneration and stability of the nanosensor

In order to investigate the selectivity of the prepared nanosensor, experiments were performed with different RNA sequences, including completely un-complementary RNA, multi-base mismatched RNA, single-base mismatched RNA and target miRNA-16, and the results were provided in Fig. 4**A**. The SWV signal changes caused by non-complementary RNA, multi-base mismatched RNA, and single-base mismatched RNA are ~1%, ~10%, and 30% of target RNA signal, respectively, indicating that the prepared nanosensor has good selectivity. To further test the selectivity of SAuNWE-based nanosensor, two common co-existing miRNA in real samples, miRNA-15 and miRNA-21, have been used to hybridize with nanosensor and the results are provided in Fig. 4**B**. From Fig. 4**B**, it can be obtained that the

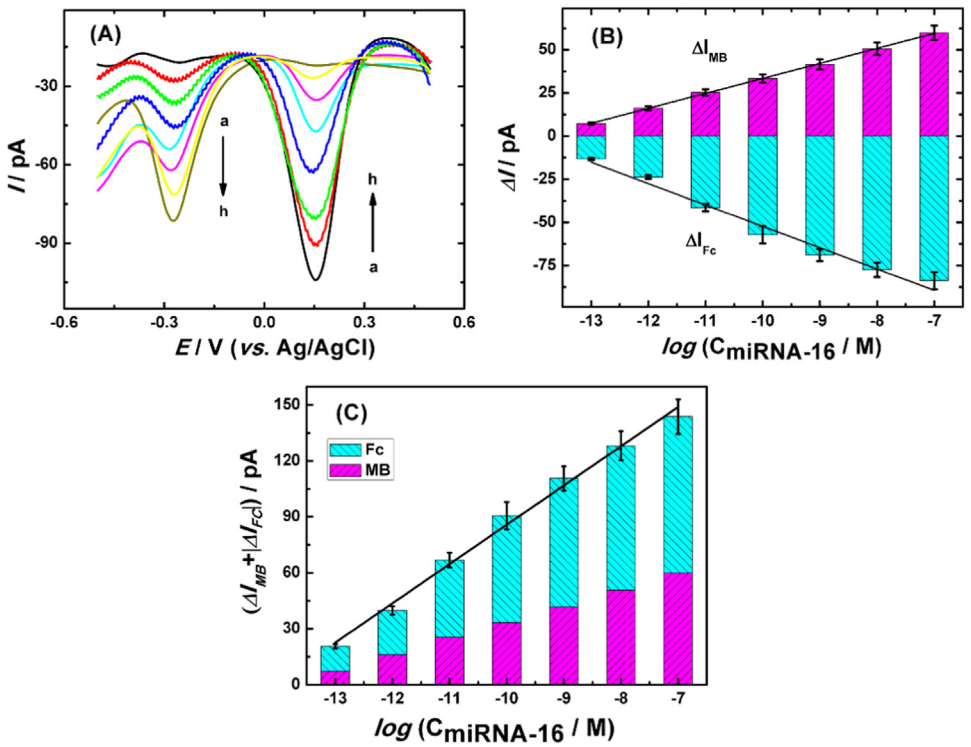

Fig. 3. (A) SWV responses of **Fc-CP-16**/**MB-CP**/SAuNWE for different concentration of miRNA-16. Concentrations (a to h): 0 fM, 0.1 pM, 1.0 pM, 10 pM, 100 pM, 1.0 nM, 10 nM, 100 nM. (B) The linear fit plots of Fc and MB signals as functions of the logarithm of target (miRNA-16) concentrations from 0.1 pM to 100 nM. (C) The linear fit plot of ΔI (ΔI_{MB} + $|\Delta I_{Fc}|$) and the logarithm of target (miRNA-16) concentrations from 0.1 pM to 100 nM. Radius, 25 ± 3 nm; length, 43 ± 4 nm.

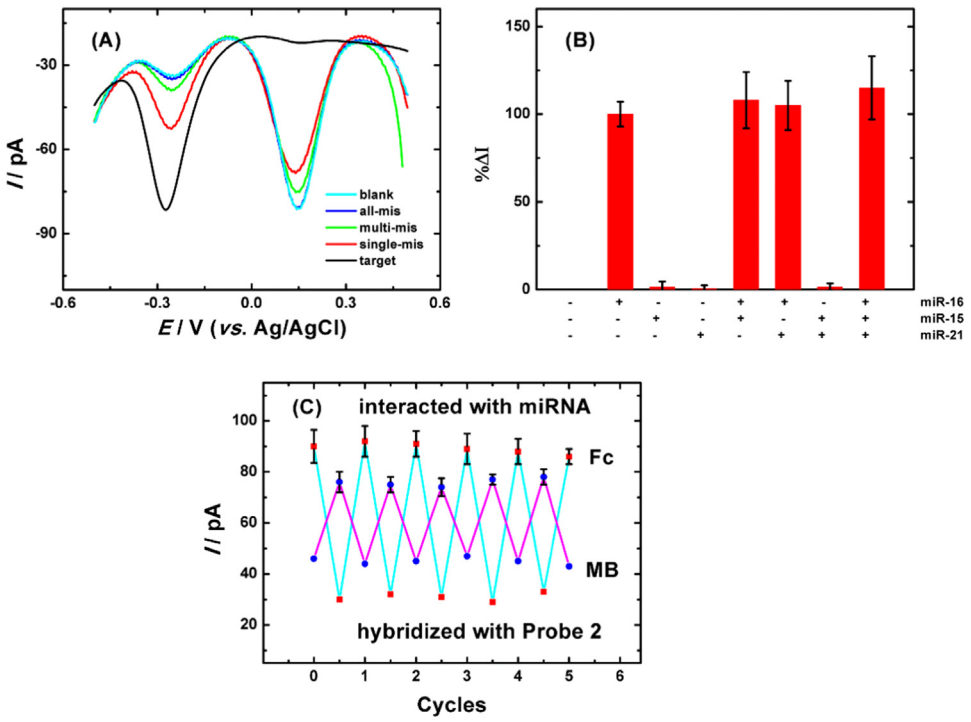

Fig. 4. (A) Specificity investigation of the nanosensor for the noncomplementary miRNA (blue curve), multi-base mismatched miRNA (green curve), single-base mismatched miRNA (red curve), and target miRNA-16 (black curve), respectively. miRNA concentrations of different base sequences are 100 nM. (B) Specificity investigation of the nanosensor for common co-existing miRNA, including miRNA-15 and miRNA-21. (C) Regeneration of the nanosensor with the stepwise interaction with miRNA-16 and then hybridization with **Fc-CP-16**. All the miRNA concentrations mentioned here, including different base sequences, miRNA-15 and miRNA-21, are 100 nM. Radius, 28 ± 6 nm, length, 41 ± 4 nm (For interpretation of the references to color in this figure legend, the reader is referred to the web version of this article.).

changes of SWV signal for miRNA-15 and miRNA-21 are ~ 1.5% and ~ 0.5%, respectively, indicating that both of co-existing miRNAs have little effect on target detection in matrix samples and the nanosensor should have potential applications for real samples analysis.

The reproducibility of the sensor is an important index to evaluate the performance of the sensor, which determines whether the sensor can be reused. Fig. 4**C** gives the SWV signals of Fc and MB in 5 hybridization/regeneration cycles. From Fig. 4**C**, it can be observed that there has only ~10% signal change after 5 hybridization/regeneration cycles, which may be due to the degradation of the immobilized MCH and this defect can be solved by use of thiolate-compounds. Subsequently, the stability of the SAuNWE-based nanosensor has also been investigated by recording SWV signal in PBS solution for seven consecutive days and the result is provided in Fig. S7 (Supporting information). After the test, the nanosensor has been stored in a refrigerator at 4 °C. It can be seen that there has only slight decrease of the SWV signals of Fc and MB and the signal of the seventh day still retains 93.3% of the original value, indicating that the stability of our sensor is good.

3.5. Real samples analysis

To evaluate the applicability of SAuNWE-based nanosensor in real samples, miRNA-16 expression level in MCF-7 cells was determined by our approach. From the results in Fig. S8, we can obtain that the miRNA-16 concentrations of the MCF-7 cell lysates 1000 cells, 10,000 cells and 100,000 cells are 0.20 pM, 2.2 pM, and 22 pM, respectively. On the basis of the aforementioned linear regression equation, the amount of miRNA-16 detected in MCF-7 cells (normal expression of miRNA-16 (Poehlmann and Sprinzl, 2010)) is approximately 820 molecules per cell, which is in good accordance with other literature (Yang et al., 2014; Zhang et al., 2013). The reliability of our method was also tested by the recovery experiments which were carried out by adding miRNA-16 with different concentrations into MCF-7 Total miRNA Extract Samples (shown in Table S3). From Table S3, it can be obtained that the recoveries for the spiked miRNA-16 with the concentration of 2.0 pM, 4.0 pM, 6.0 pM and 8.0 pM are 105.0%, 97.5%, 96.7% and 102.5%, and the relative standard deviations are 4.3%, 2.3%, 3.4% and 2.7%, respectively. These results have indicated that the nanosensors can be potentially applied to the sensitive detection of miRNA-16 in real samples.

4. Conclusions

In summary, on the basis of the novel dual-signaling amplification strategy, a new electrochemical aptamer-based “signal-on/off” biosensor for the detection of miRNA has been developed by use of SAuNWEs. The prepared nanosensor has relatively wide linear range (0.1 pM to 100 nM), high sensitivity (LOD, 16 fM) and good selectivity. Although this nanosensor had only been used for the detection of miRNA-16 expression level in MCF-7 cells. Considering its small overall dimension, we believe that our new analytical method will have promising applications in the sensitive and selective electrochemical determination of other small molecules and proteins in living system.

CRediT authorship contribution statement

Haoran Tang: Data curation, Methodology, Writing - original draft. **Jiahui Zhu:** Conceptualization, Data curation, Methodology. **Dongmei Wang:** Investigation, Methodology. **Yongxin Li:** Conceptualization, Funding acquisition, Supervision, Writing - review & editing.

Acknowledgments

We thank Prof. Bo Zhang (University of Washington) for his useful suggestions and discussion. This work is financially supported by the National Natural Science Foundation of China (No. 21775003, No. 21375002), the Foundation of Innovation Team of Bioanalytical Chemistry of Anhui Province.

Supplementary material

Supplementary Material as noted in the text. This material is available free of charge via the Internet.

Declaration of interests

None.

Appendix A. Supporting information

Supplementary data associated with this article can be found in the online version at doi:10.1016/j.bios.2019.02.023.

References

Actis, P., Tokar, S., Clausmeyer, J., Babakinejad, B., Mikhaleva, S., Cornut, R., Takahashi, Y., Cordoba, A.L., Novak, P., Shevchuck, A.I., Dougan, J.A., Kazarian, S.G., Gorelkin, P.V., Erofeev, A.S., Yaminsky, I.V., Unwin, P.R., Schuhmann, W., Klenerman, D., Rusakov, D.A., Sviderskaya, E.V., Korchev, Y.E., 2014. ACS Nano 8 (1), 875–884.

Bard, A.J., Faulkner, L.R., 2001. Electrochemical Methods. John Wiley & Sons, New York.

Chen, X., Ba, Y., Ma, L., Cai, X., Yin, Y., Wang, K., Guo, J., Zhang, Y., Chen, J., Guo, X., Li, Q., Li, X., Wang, W., Zhang, Y., Wang, J., Jiang, X., Xiang, Y., Xu, C., Zheng, P., Zhang, J., Li, R., Zhang, H., Shang, X., Gong, T., Ning, G., Wang, J., Zen, K., Zhang, J., Zhang, C.-Y., 2008. Cell Res. 18 (10), 997–1006.

Chidsey, C.E.D., Bertozzi, C.R., Putvinski, T.M., Mujsce, A.M., 1990. J. Am. Chem. Soc. 112 (11), 4301–4306.

Coulouarn, C., Factor, V.M., Andersen, J.B., Durkin, M.E., Thorgeirsson, S.S., 2009. Oncogene 28 (40), 3526–3536.

Deng, C., Pi, X., Qian, P., Chen, X., Wu, W., Xiang, J., 2017. Anal. Chem. 89 (1), 966–973.

Dong, H., Lei, J., Ding, L., Wen, Y., Ju, H., Zhang, X., 2013. Chem. Rev. 113 (8), 6207–6233.

Eksin, E., Erdem, A., 2018. J. Electroanal. Chem. 810, 232–238.

Erdem, A., Congur, G., 2014. Talanta 118, 7–13.

Feng, Q., Wang, M., Zhao, X., Wang, P., 2018. Langmuir 34 (34), 10153–10162.

Frascella, F., Ricciardi, S., Pasquardini, L., Potrich, C., Angelini, A., Chiado, A., Pederzolli, C., De Leo, N., Rivolo, P., Pirri, C.F., Descrovi, E., 2015. Analyst 140 (16), 5459–5463.

Gao, T., Zhi, J., Mu, C., Gu, S., Xiao, J., Yang, J., Wang, Z., Xiang, Y., 2018. Talanta 178, 89–93.

Hua, H., Liu, Y., Guan, X., Li, Y., 2018a. Microchim. Acta 185 (2).

Hua, H., Liu, Y., Wang, D., Li, Y., 2018b. Anal. Chem. 90 (16), 9677–9681.

Jena, B.K., Percival, S.J., Zhang, B., 2010. Anal. Chem. 82 (15), 6737–6743.

Kakkassery, V., Schroers, R., Coupland, S.E., Wunderlich, M.-I., Schargus, M., Heinz, C., Wasmuth, S., Heiligenhaus, A., Ahle, G., Lenoble, P., Schlegel, U., Schmiegel, W., Dick, H.B., Baraniskin, A., 2017. Blood 129 (23), 3130–3133.

Katemann, B.B., Schuhmann, W., 2002. Electroanalysis 14 (1), 22–28.

Laterza, O.F., Lim, L., Garrett-Engele, P.W., Vlasakova, K., Muniappa, N., Tanaka, W.K., Johnson, J.M., Sina, J.F., Fare, T.L., Sistare, F.D., Glaab, W.E., 2009. Clin. Chem. 55 (11), 1977–1983.

Li, Y., Bergman, D., Zhang, B., 2009. Anal. Chem. 81 (13), 5496–5502.

Li, Y., Hu, K., Yu, Y., Rotenberg, S.A., Amatore, C., Mirkin, M.V., 2017. J. Am. Chem. Soc. 139 (37), 13055–13062.

Li, Y., Wu, Q., Jiao, S., Xu, C., Wang, L., 2013. Anal. Chem. 85 (8), 4135–4140.

Liu, C.G., Calin, G.A., Meloon, B., Gamliel, N., Sevignani, C., Ferracin, M., Dumitru, C.D., Shimizu, M., Zupo, S., Dono, M., Alder, H., Bullrich, F., Negrini, M., Croce, C.M., 2004. Proc. Natl. Acad. Sci. USA 101 (26), 9740–9744.

Liu, J.L., Tang, Z.L., Zhuo, Y., Chai, Y.Q., Yuan, R., 2017. Anal. Chem. 89 (17), 9108–9115.

Liu, Y., Li, M., Zhang, F., Zhu, A., Shi, G., 2015. Anal. Chem. 87 (11), 5531–5538.

Marquitan, M., Clausmeyer, J., Actis, P., Cordoba, A.L., Korchev, Y., Mark, M.D., Herlitze, S., Schuhmann, W., 2016. Chemelectrochem 3 (12), 2125–2129.

Miao, X., Cheng, Z., Ma, H., Li, Z., Xue, N., Wang, P., 2018. Anal. Chem. 90 (2), 1098–1103.

Poehlmann, C., Sprinzl, M., 2010. Anal. Chem. 82 (11), 4434–4440.

Qian, R.C., Cao, Y., Long, Y.T., 2016. Anal. Chem. 88 (17), 8640–8647.

Salamifar, S.E., Lai, R.Y., 2014. Anal. Chem. 86 (6), 2849–2852.

Sassolas, A., Leca-Bouvier, B.D., Blum, L.J., 2008. Chem. Rev. 108 (1), 109–139.

Schetter, A.J., Leung, S.Y., Sohn, J.J., Zanetti, K.A., Bowman, E.D., Yanaihara, N., Yuen, S.T., Chan, T.L., Kwong, D.L.W., Au, G.K.H., Liu, C.-G., Calin, G.A., Croce, C.M., Harris, C.C., 2008. JAMA-J. Am. Med. Assoc. 299 (4), 425–436.

Shao, Y.H., Mirkin, M.V., Fish, G., Kokotov, S., Palanker, D., Lewis, A., 1997. Anal. Chem. 69 (8), 1627–1634.

Shi, K., Dou, B.T., Yang, C.Y., Chai, Y.Q., Yuan, R., Xiang, Y., 2015. Anal. Chem. 87 (16), 8578–8583.

Sun, P., Mirkin, M.V., 2008. J. Am. Chem. Soc. 130 (26), 8241–8250.

Thomson, J.M., Parker, J., Perou, C.M., Hammond, S.M., 2004. Nat. Methods 1 (1), 47–53.

Velmurugan, J., Sun, P., Mirkin, M.V., 2009. J. Phys. Chem. C 113 (1), 459–464.

Wang, D., Xiao, X., Xu, S., Liu, Y., Li, Y., 2018a. Biosens. Bioelectron. 99, 431–437.

Wang, H., Gong, Y., Li, Y., 2018b. Electrochem. Commun. 86, 63–67.

Wang, T., Viennois, E., Merlin, D., Wang, G., 2015. Anal. Chem. 87 (16), 8173–8180.

Wang, Y., Noel, J.-M., Velmurugan, J., Nogala, W., Mirkin, M.V., Lu, C., Collignon, M.G., Lemaitre, F., Amatore, C., 2012. Proc. Natl. Acad. Sci. USA 109 (29), 11534–11539.

Weiss, F.U., Marques, I.J., Woltering, J.M., Vlecken, D.H., Aghdassi, A., Partecke, L.I., Heidecke, C.-D., Lerch, M.M., Bagowski, C.P., 2009. Gastroenterology 137 (6), 2136–2145.

Wu, L., Zhang, X., Liu, W., Xiong, E., Chen, J., 2013. Anal. Chem. 85 (17), 8397–8402.

Xiang, J., Pi, X., Chen, X., Xiang, L., Yang, M., Ren, H., Shen, X., Qi, N., Deng, C., 2017. Biosens. Bioelectron. 96, 268–274.

Yang, C.Y., Dou, B.T., Shi, K., Chai, Y.Q., Xiang, Y., Yuan, R., 2014. Anal. Chem. 86 (23), 11913–11918.

Yu, S., Wang, Y.Y., Jiang, L.P., Bi, S., Zhu, J.J., 2018. Anal. Chem. 90 (7), 4544–4551.

Yuen, T., Wurmbach, E., Pfeffer, R.L., Ebersole, B.J., Sealfon, S.C., 2002. Nucleic Acids Res. 30 (10).

Zhang, B., Zhang, Y.H., White, H.S., 2004. Anal. Chem. 76 (21), 6229–6238.

Zhang, B., Zhang, Y.H., White, H.S., 2006. Anal. Chem. 78 (2), 477–483.

Zhang, M., Liu, Y.-Q., Yu, C.-Y., Yin, B.-C., Ye, B.-C., 2013. Analyst 138 (17), 4812–4817.

Zhang, Y., Xu, S., Qian, Y., Yang, X., Li, Y., 2015. RSC Adv. 5 (94), 77248–77254.

Zhang, Y., Xu, S., Xiao, X., Liu, Y., Qian, Y., Li, Y., 2017. Chem. Commun. 53 (19), 2850–2853.